

Supporting Information

Towards Robust Hydrogen Evolution Electrocatalysts in Immiscible Copper–Molybdenum Alloys by Amorphization

Long Chen^{a, #}, Xiying Jian^{a, #}, Qingsheng Gao^b, Zhijie Cao^c, Zibo Chen^{d, **}, Huai-Jun
Lin^{a, *}

^a Institute of Advanced Wear & Corrosion Resistance and Functional Materials,
Jinan University, Guangzhou 510632, PR China

^b Department of Chemistry, Jinan University, Guangzhou, 510632, PR China

^c College of physics, Ningxia University, Ningxia, Yinchuan, 750021, PR China

^d Institute of Chemical & process engineering, University of Strathclyde, Glasgow G4
0JQ, UK

Both authors contributed equally to this work

* Corresponding author, Email: hjlin@jnu.edu.cn

** Corresponding author, Email: zibo.chen@strath.ac.uk

I. Supplementary Texts

1. Preparation Materials.

Chemicals. The targets used for magnetron sputtering were purchased from ZhongNuo Advanced Material (Beijing) Technology Co., Ltd. The nickel foam was purchased from Kunshan Guangjiayuan New Material Co., Ltd. Potassium hydroxide (KOH, 85%), sulfuric acid (H₂SO₄, 98%), hydrochloric acid (HCl, 36~38 wt.%), acetone (99.5%) and absolute ethanol were obtained from the Guangzhou Chemical Reagent Factory. All chemicals were analytical grade and were used as received without any treatment. Throughout the experiments, deionized water (resistance > 18 M cm) was used.

Synthesis of Cu_xMo_y catalysts on NF. The Cu_xMo_y (atomic ratio from 28:72 to 85:15) catalysts were prepared using a direct current (DC) magnetron sputtering apparatus (SuPro Instruments 300 plus) onto a nickel foam substrate. Prior to the magnetron sputtering experiments, the Ni foam (NF) was subjected to a series of cleaning procedures, including ultrasonication with acetone, dilute hydrochloric acid, deionized water and absolute ethanol. Subsequently, the NF was subjected to a drying process in a vacuum chamber at a temperature of 60°C. The targets underwent a pre-sputtering process for 10 minutes to eliminate surface contaminants before sputtering. In order to achieve uniform sputtering, the rotating tray speed was set at 10 r/min. The complete catalyst sample was prepared by sputtering both sides of the nickel foam. Similarly, the alloys were deposited onto a polymer film for X-ray diffraction (XRD) analysis.

2. Materials characterization

The X-ray diffractometer (XRD, Rigaku Ultima IV) was employed to analyze the phases of the Cu_xMo_y alloys. Scanning electron microscopy (SEM, Ultra-55) and transmission electron microscopy (TEM, FEI Talos F200X) were employed to investigate the morphology and spatial structure of the samples. Energy Dispersive X-

ray spectroscopy (EDS) elemental mapping images were obtained during SEM measurements. Raman spectra were obtained using the HORIBA LabRAM HR Evolution ($\lambda = 532$ nm). The valence state information of the Cu_xMo_y alloys was tested using X-ray photoelectron spectroscopy (XPS, Thermo Scientific K-Alpha⁺) with a monochromatic Al K α source (1486.6 eV). The XPS spectra were subjected to charge correction based on the binding energy standard of C 1s = 284.8 eV. The Cu LMM spectra were applied to facilitate the valence analysis. In particular, the Cu_xMo_y alloys mentioned in this paper were expressed in nominal composition and confirmed by EDS results.

3. Electrochemical measurements

All electrochemical measurements were conducted in a three-electrode system on an electrochemical workstation (CH Instruments, 760E). The typical cell consisted of three electrodes: a Cu_xMo_y working electrode, a graphite rod counter electrode and a Hg/HgO or saturated calomel electrode (SCE) reference electrode. The electrolyte solution employed in this work comprises 1.0 M KOH and 0.5 M H_2SO_4 . All measured potentials against the reference electrode are corrected to potentials against the reversible hydrogen electrode (RHE) based on the results of calibration experiments (**Fig. S24**). Linear sweep voltammetry (LSV) test was performed at a rate of 5 mV s^{-1} following 30 cycles of cyclic voltammetry (CV) activation scanning. It is worth noting that, unless otherwise stated, all LSV curves mentioned in this work were 90% iR compensated. To estimate the electrochemically active surface area (ECSA) of the Cu_xMo_y electrodes, double-layer capacitance (C_{dl}) values were obtained by a series of CV investigations with six scan rates (30, 60, 90, 120, 150 and 180 mV/s) in the non-Faradaic range. Unless otherwise stated, electrochemical impedance spectroscopy (EIS) was conducted with an amplitude voltage of 10 mV from 0.01 to 10^5 Hz at -0.1 V (V vs. RHE). The linear parts of the Tafel plots were derived by means of the application of the Tafel equation ($\eta = b \log j + a$, where j is the current density and b is the Tafel slope). To evaluate the stability of the as-prepared catalysts, chronoamperometric and chrono potentiometric measurements were performed. The

underpotentially deposited hydrogen (H_{upd}) desorption peaks of the Cu_xMo_y alloys were investigated through the use of CV curves within a potential range of -0.1 to 0.3 V (V vs. RHE). The peak in the potential range of $0.60 < E < 1.00$ V (V vs. RHE) is associated with the adsorption of OH,^{1,2} and the potential range of 0.50 to 1.10 V (V vs. RHE) is employed for the CV test.

II. Supplementary Figures and Tables

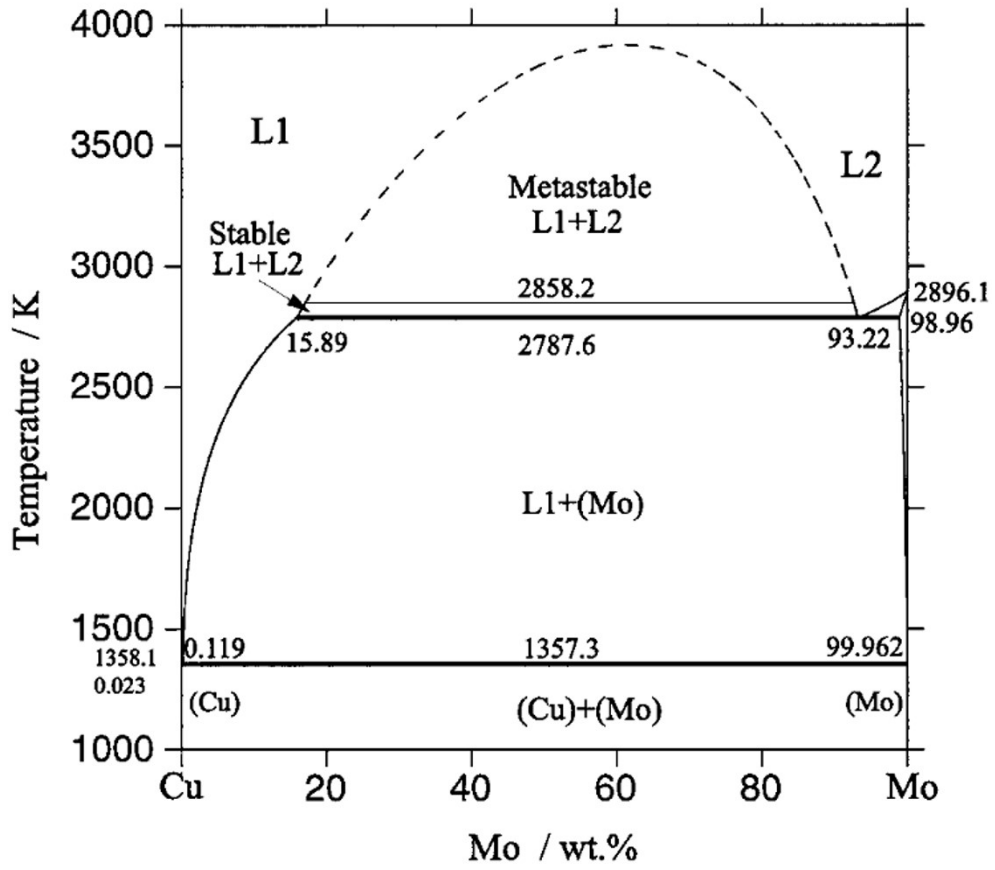


Fig. S1. Calculated Cu-Mo binary phase diagram.³

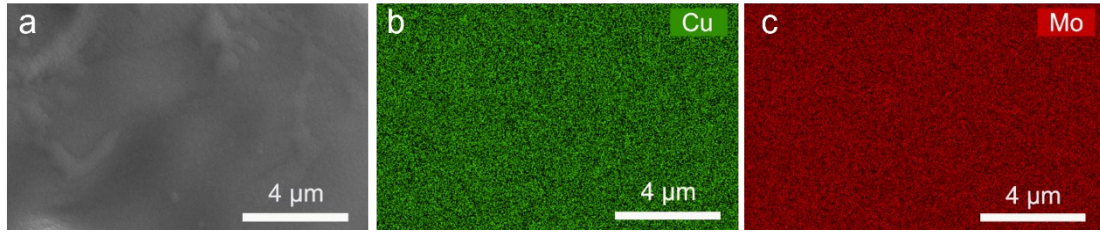


Fig. S2. (a) Surface SEM image of the Cu₅₀Mo₅₀ alloy. (b and c) Corresponding EDS mappings.

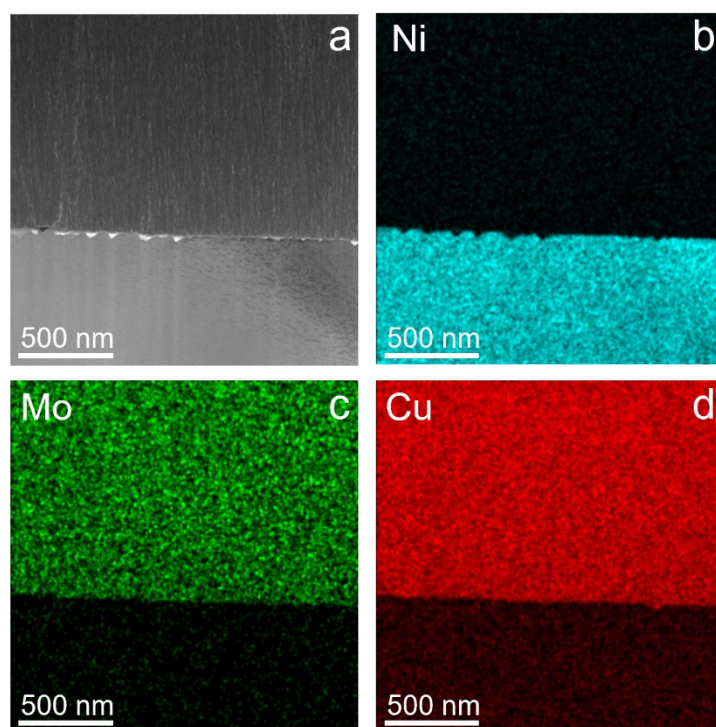


Fig. S3. (a) Cross-sectional image and (b–d) corresponding EDS mappings of the $\text{Cu}_{50}\text{Mo}_{50}$ alloy.

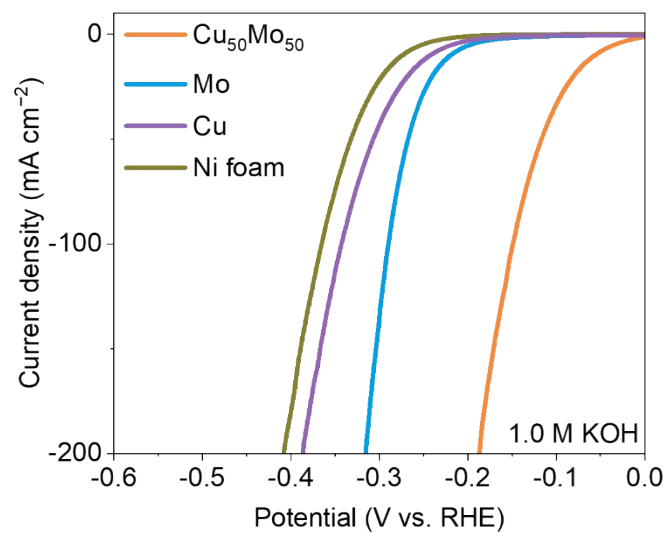


Fig. S4. LSV curves of the Cu₅₀Mo₅₀ alloy, Mo, Cu and Ni foam in 1.0 M KOH.

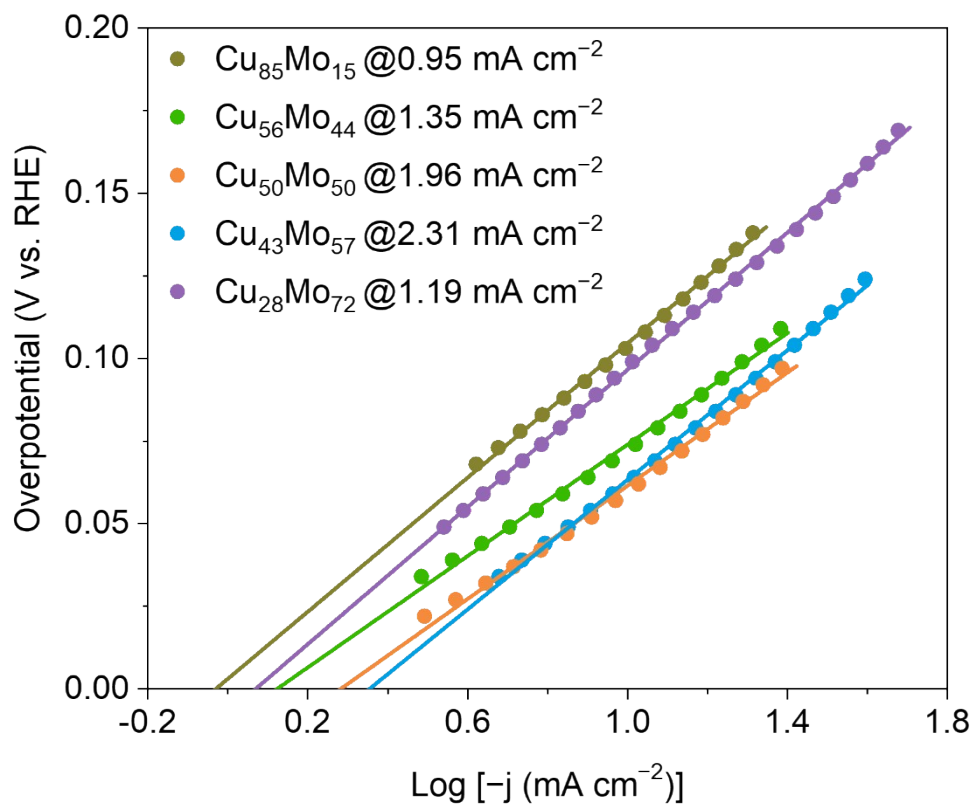


Fig. S5. The exchange current densities of the Cu_xMo_y alloys in 1.0 M KOH.

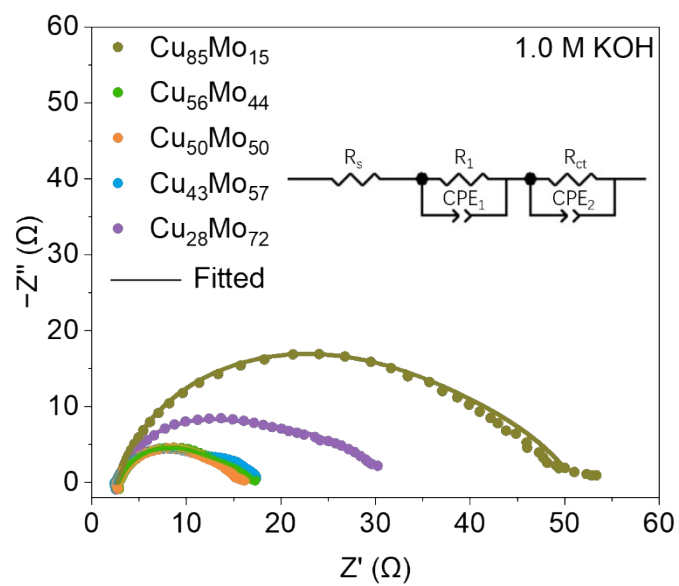


Fig. S6. Fitting of the Nyquist plots of the Cu_xMo_y alloys in 1.0 M KOH.

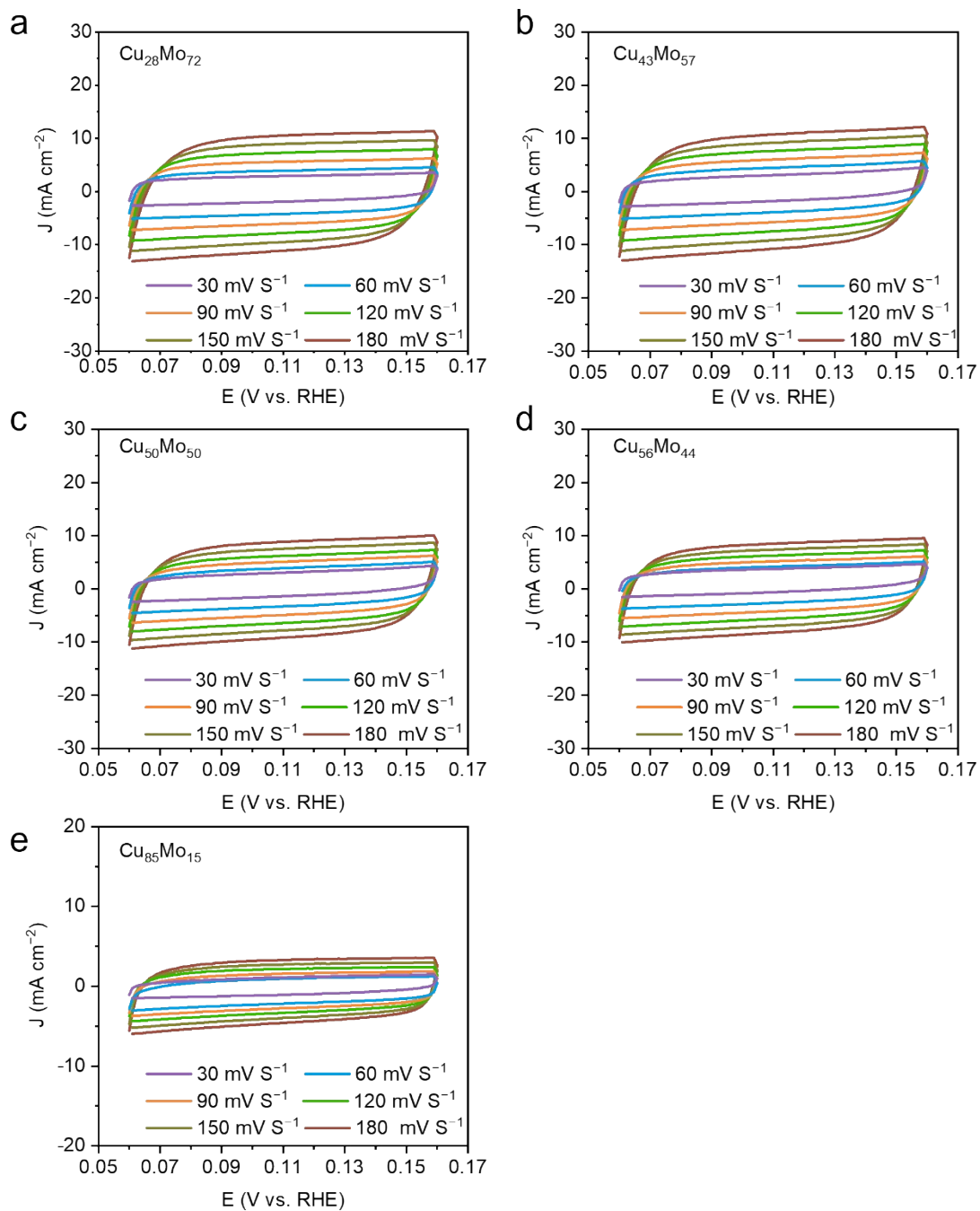


Fig. S7. CV curves in the non-Faradaic region with different scan rates (30, 60, 90, 120, 150, 180 mV s⁻¹) over (a) $\text{Cu}_{28}\text{Mo}_{72}$, (b) $\text{Cu}_{43}\text{Mo}_{57}$, (c) $\text{Cu}_{50}\text{Mo}_{50}$, (d) $\text{Cu}_{56}\text{Mo}_{44}$ and (e) $\text{Cu}_{85}\text{Mo}_{15}$ alloys in 1.0 M KOH.

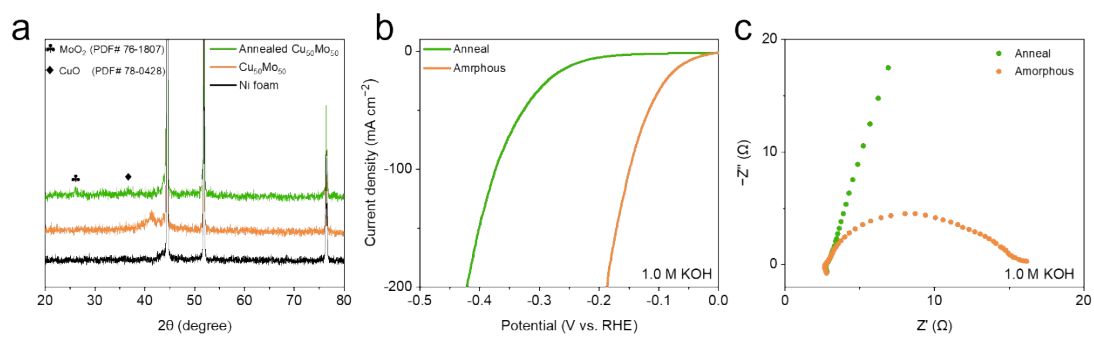


Fig. S8. Structural characterization and alkaline electrochemical properties of the $\text{Cu}_{50}\text{Mo}_{50}$ alloy before and after annealing at 500°C . (a) XRD patterns. (b) LSV curves. (c) Nyquist plots.

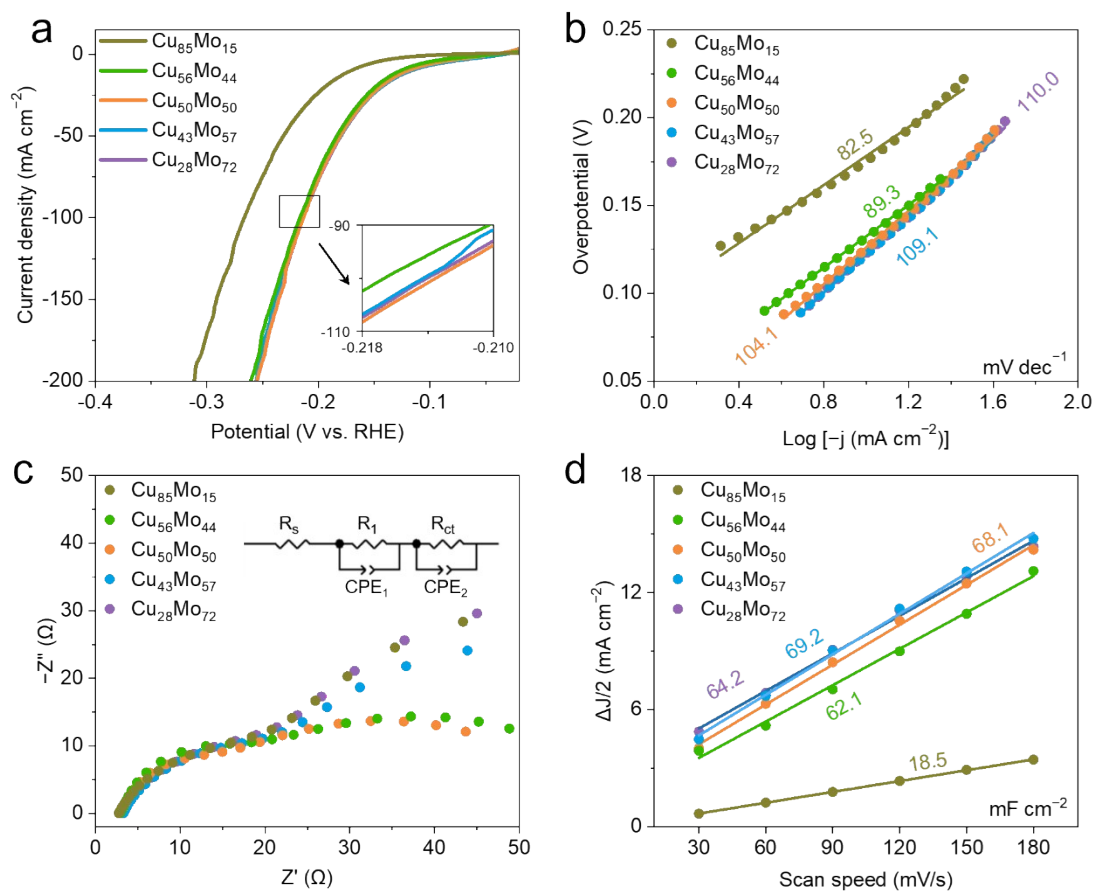


Fig. S9. HER performance of the Cu_xMo_y alloys in 0.5 M H₂SO₄. (a) LSV curves. (b) Tafel plots. (c) Nyquist plots. (d) $\Delta J/2$ of the Cu_xMo_y plotted against scan rates.

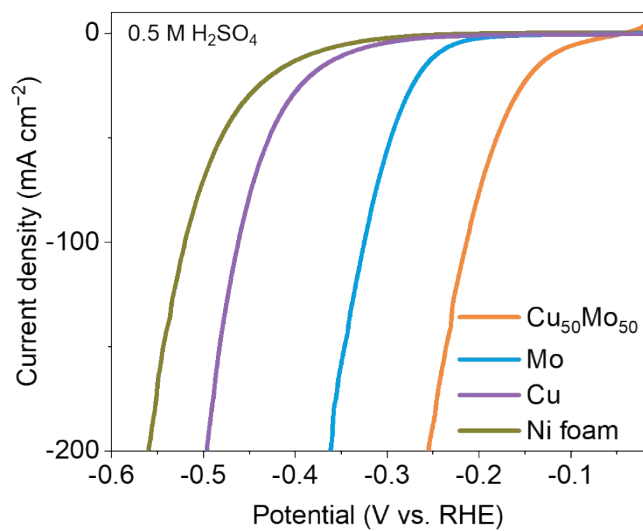


Fig. S10. LSV curves of the Cu₅₀Mo₅₀ alloy, Mo, Cu and Ni foam in 0.5 M H₂SO₄.

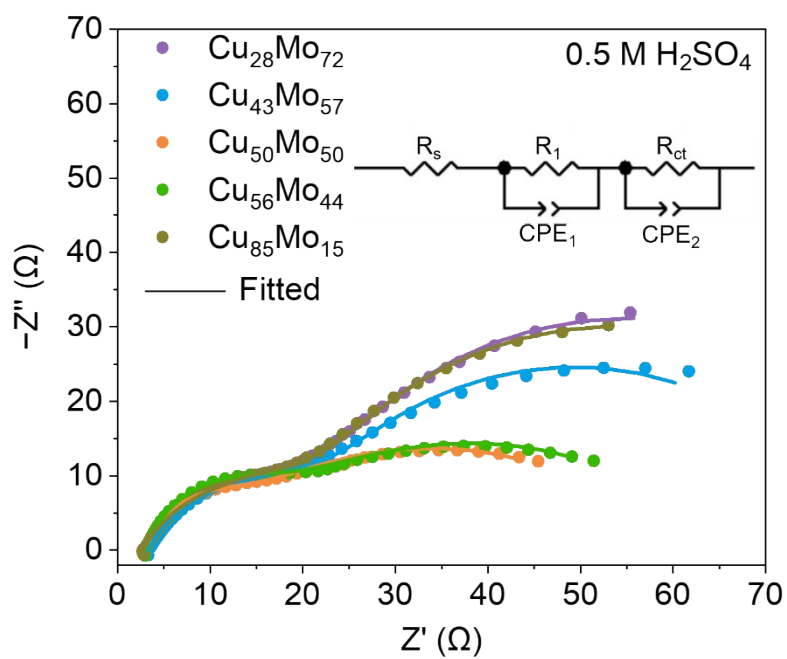


Fig. S11. Fitting of the Nyquist plots of the Cu_xMo_y alloys in 0.5 M H₂SO₄.

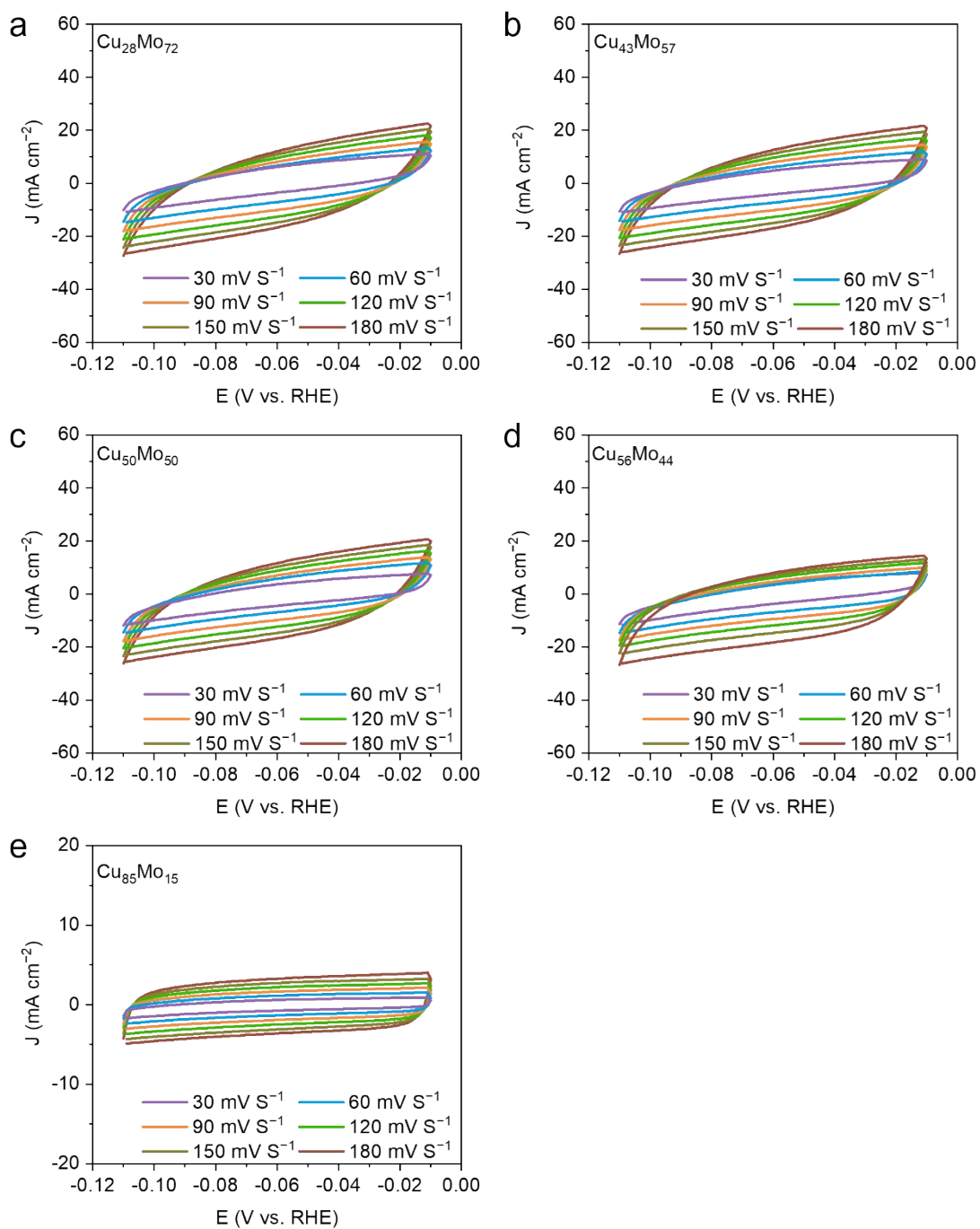


Fig. S12. CV curves in the non-Faradaic region with different scan rates (30, 60, 90, 120, 150, 180 mV s⁻¹) over (a) $\text{Cu}_{28}\text{Mo}_{72}$, (b) $\text{Cu}_{43}\text{Mo}_{57}$, (c) $\text{Cu}_{50}\text{Mo}_{50}$, (d) $\text{Cu}_{56}\text{Mo}_{44}$ and (e) $\text{Cu}_{85}\text{Mo}_{15}$ alloys in 0.5 M H₂SO₄.

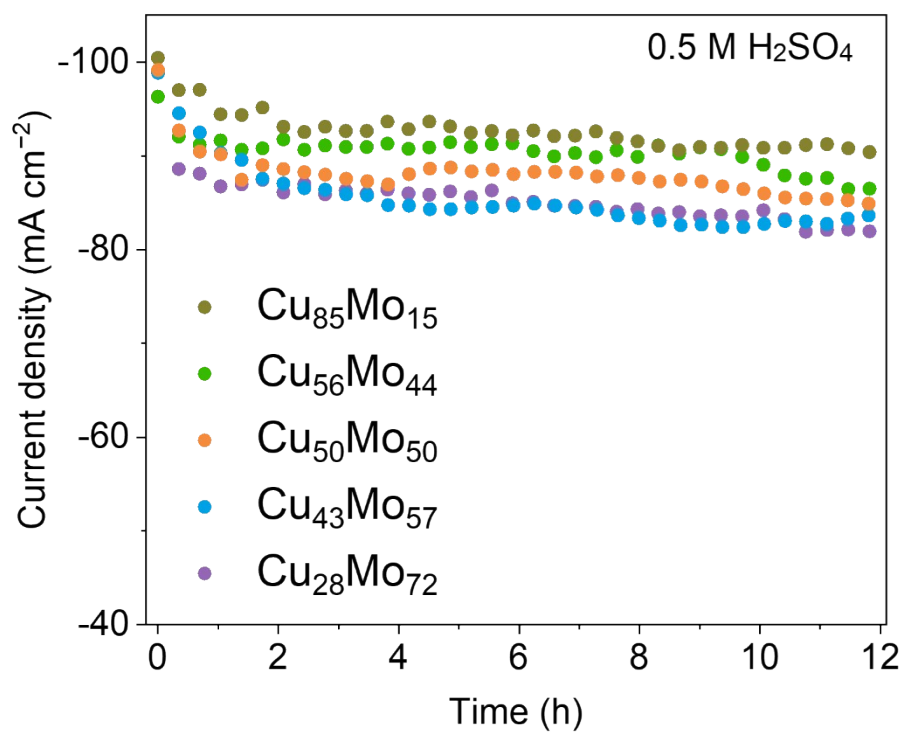


Fig. S13. Chronoamperometric tests of the Cu_xMo_y alloys at 100 mA cm⁻² in 0.5 M H₂SO₄.

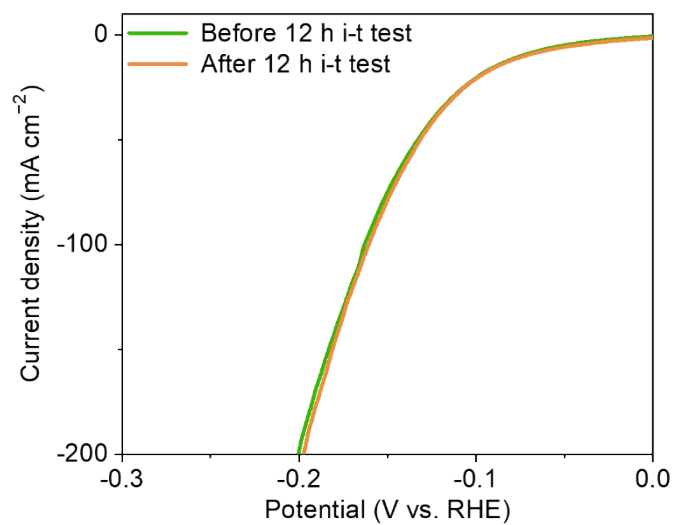


Fig. S14. LSV curves of the Cu₅₀Mo₅₀ alloy before and after the 12 h i-t test at 300 mA cm⁻² in 1.0 M KOH.

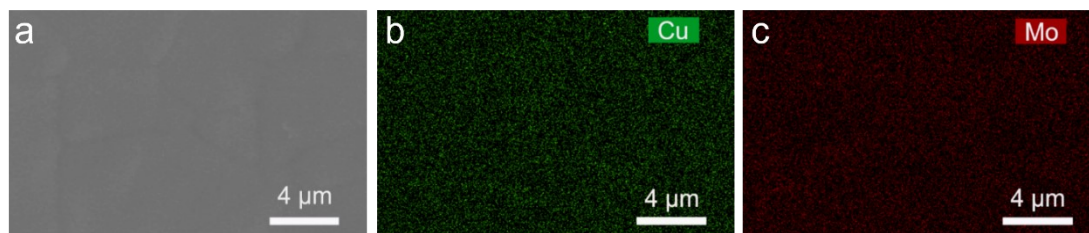


Fig. S15. (a–c) EDS mappings of the $\text{Cu}_{50}\text{Mo}_{50}$ alloy after the 12 h i-t test at 300 mA cm^{-2} in 1.0 M KOH.

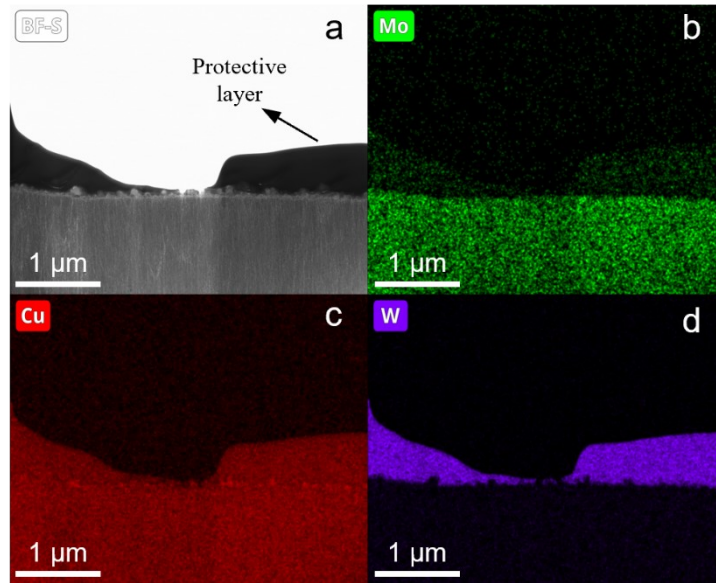


Fig. S16. (a-d) Cross-sectional EDS mappings of the amorphous $\text{Cu}_{50}\text{Mo}_{50}$ alloy after 12 h i-t test at 300 mA cm^{-2} .

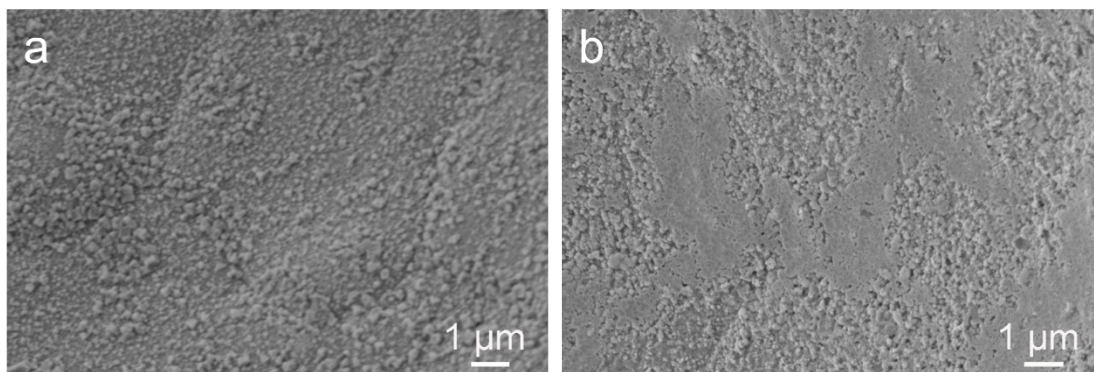


Fig. S17. SEM images of the amorphous $\text{Cu}_{50}\text{Mo}_{50}$ alloy after i-t tests at 300 mA cm^{-2} in 1.0 M KOH. (a) 12 h. (b) Long term i-t.

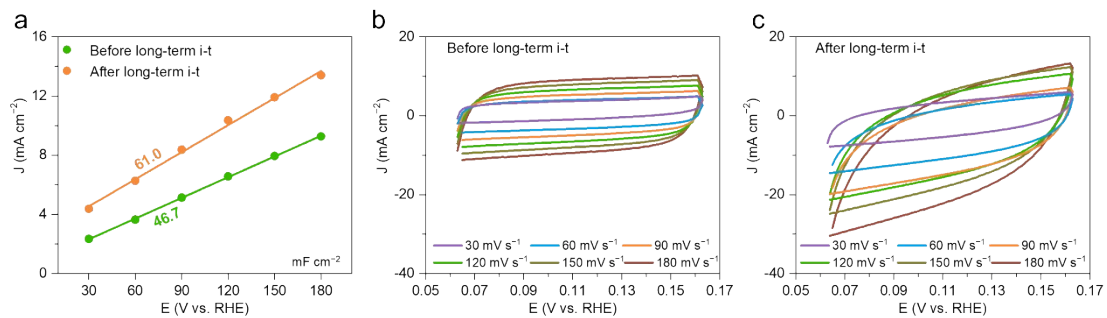


Fig. S18. (a) C_{dl} before and after the long-term $i-t$ test at 300 mA cm⁻² in 1.0 M KOH. CV curves in the non-Faradaic region with different scan rates over $\text{Cu}_{50}\text{Mo}_{50}$ (b) before and (c) after long-term $i-t$ test.

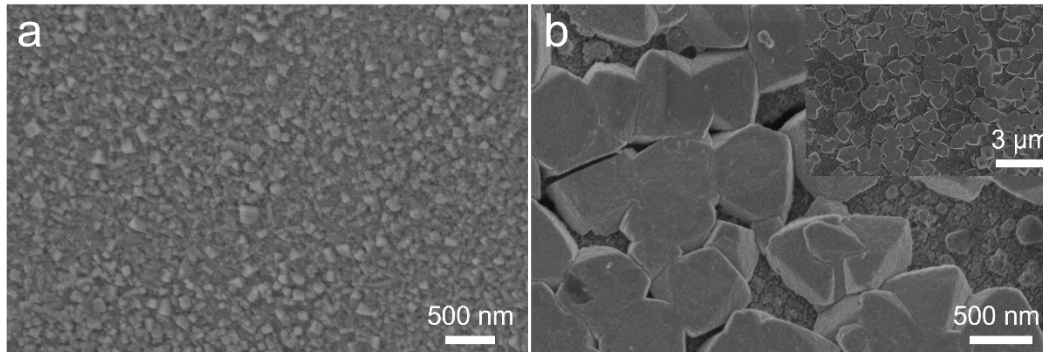


Fig. S19 SEM images of the $\text{Cu}_{50}\text{Mo}_{50}$ alloy after i-t tests at different current densities. (a) 100 mA cm^{-2} . (b) 500 mA cm^{-2} . Inset: $3 \mu\text{m}$ scale.

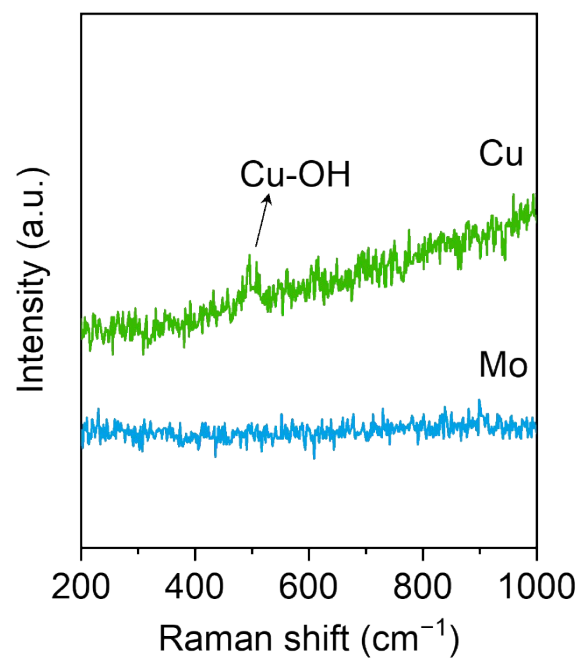


Fig. S20. Raman spectra of Cu and Mo at 0.85 V (V vs. RHE) in 1.0 M KOH.

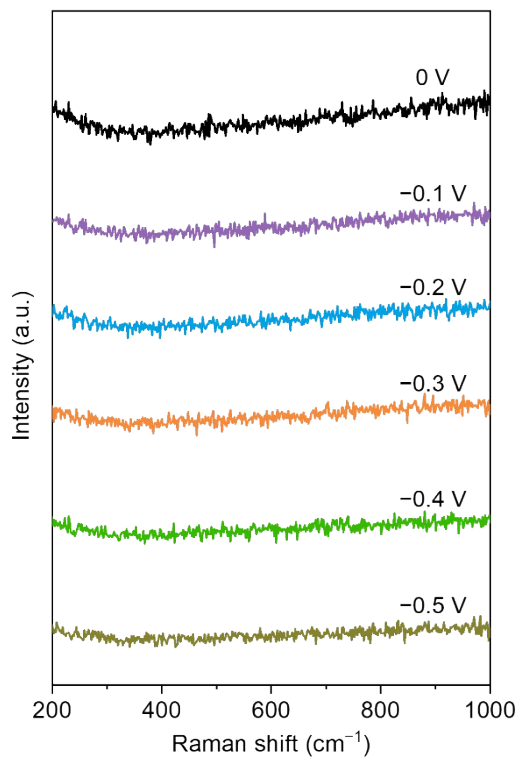


Fig. S21. In situ Raman spectra of HER for the Cu₅₀Mo₅₀ alloy at different potentials in 1.0 M KOH.

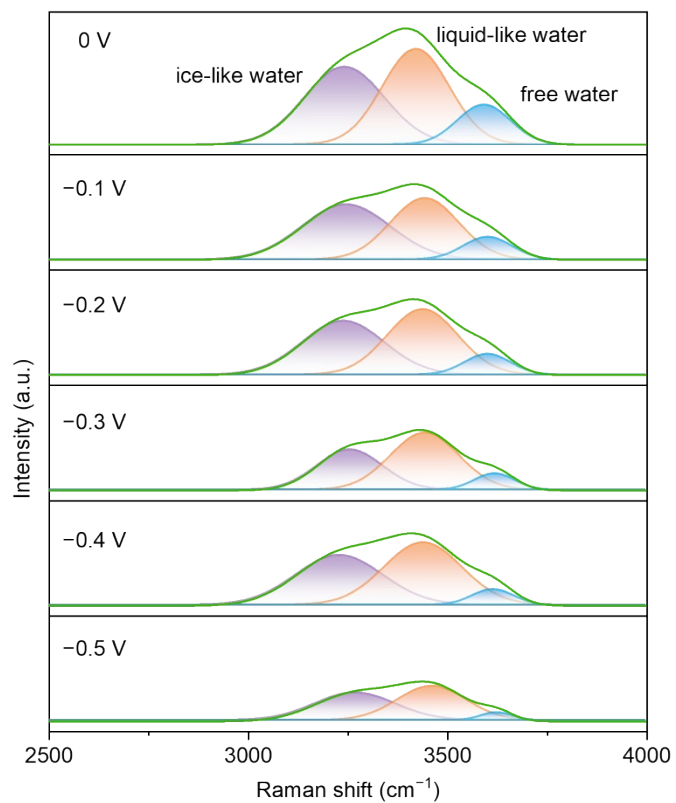


Fig. S22. The three peaks of interfacial water of the $\text{Cu}_{50}\text{Mo}_{50}$ alloy at different potentials.

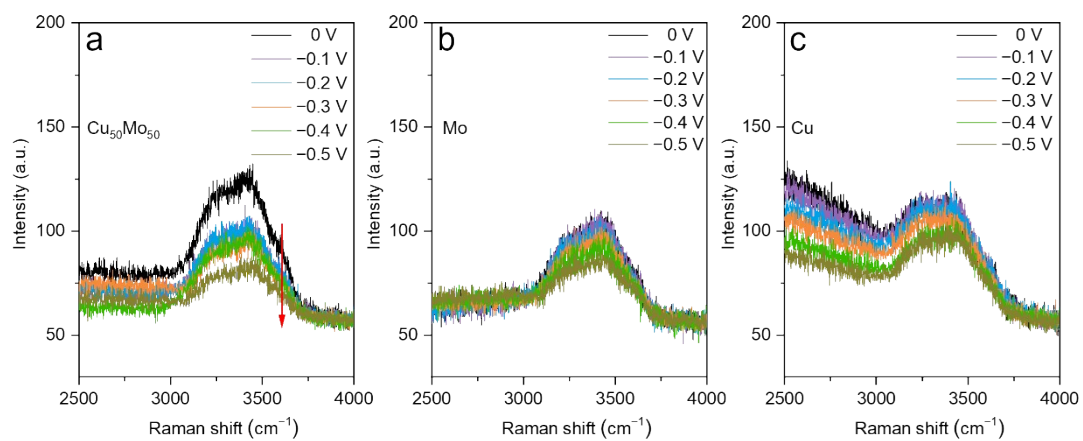


Fig. S23. In situ Raman spectra at different potentials in 1.0 M KOH. (a) Cu₅₀Mo₅₀ alloy. (b) Mo. (c) Cu.

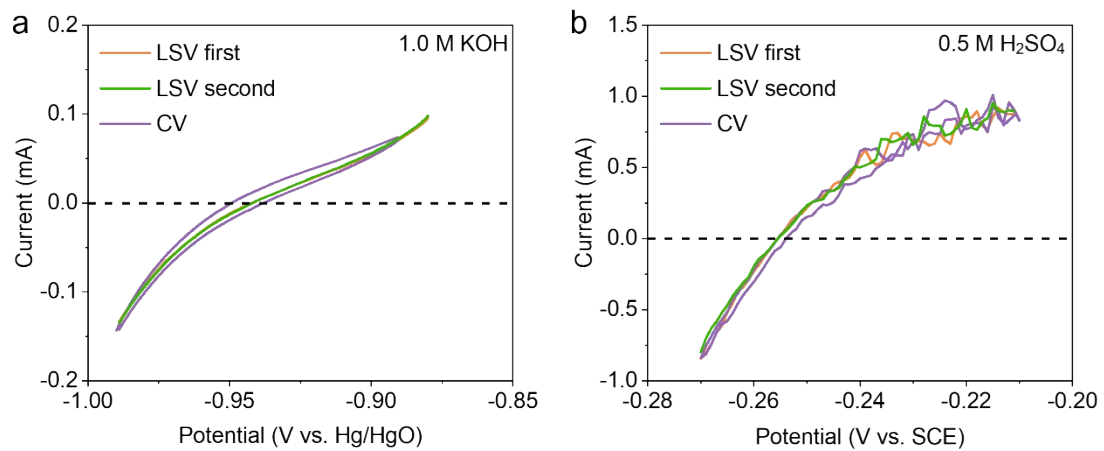


Fig. S24. The results of the RHE calibration experiments. (a) 1.0 M KOH. (b) 0.5 M H₂SO₄.

Table S1. Summary of HER performance in 1.0 M KOH electrolyte for the Cu_xMo_y alloys.

Cu_xMo_y	η_{10} (mV)	C_{dl} (mF cm ⁻²)	R_{ct} (Ω)	Tafel slope (mV dec ⁻¹)
$\text{Cu}_{85}\text{Mo}_{15}$	102	19.3	24.45	101.5
$\text{Cu}_{56}\text{Mo}_{44}$	70	41.4	7.86	84.3
$\text{Cu}_{50}\text{Mo}_{50}$	57	45.2	9.09	85.6
$\text{Cu}_{43}\text{Mo}_{57}$	60	55.4	10.88	98.0
$\text{Cu}_{28}\text{Mo}_{72}$	96	56.6	19.02	103.8

Table S2. Comparison of our work with reported HER catalysts in 1.0 M KOH.

	Catalysts	η_{10} (mV)	η_{100} (mV)	Ref.
I	MoC/Ni@NCNTs-MoC@C	-	145.9	4
II	Cu ₅₀ Mo ₅₀ @NF	57	149	This work
III	Ni _{0.8} Mo _{0.8} /NF	-	158	5
IV	Fe ₇ S ₈ /1T MoS ₂	9	162	6
V	Ni/Mo-TEC@NF	64	171	7
VI	Mo-NiP _x /NiS _y	85	173	8
VII	Co,Ni-MoB ₂ @CNT/CC	98	182.7	9
VIII	P-MoP/Mo ₂ N	89	190	10
IX	Cu ₅₀ W ₅₀ @NF	65	194	11
X	MoO ₃ -Co(OH) ₂ @Ag NWs	142	220	12
XI	NiFeP@Ni ₂ P/MoO _x	80	232	13
XII	Co,Ni-MoB ₂ /CC	114.4	250.1	9

Table S3. Summary of HER performance in 0.5 M H₂SO₄ electrolyte for the Cu_xMo_y alloys.

Cu_xMo_y	η₁₀ (mV)	C_{dl} (mF cm⁻²)	R_{ct} (Ω)	Tafel slope (mV dec⁻¹)
Cu ₈₅ Mo ₁₅	172	18.5	62.11	82.5
Cu ₅₆ Mo ₄₄	127	62.1	51.61	89.3
Cu ₅₀ Mo ₅₀	120	68.1	49.48	104.1
Cu ₄₃ Mo ₅₇	118	69.2	52.67	109.1
Cu ₂₈ Mo ₇₂	119	64.2	62.24	110.0

Table. S4 Summary of ICP results for the Cu₅₀Mo₅₀ alloy after i-t tests at different current densities.

Current density (mA cm ⁻²)	Cu concentration average (ppm)	Mo concentration average (ppm)
100	0.002	0.316
300	0.001	0.381
500	0.004	0.302

References

1. B. Mao, P. Sun, Y. Jiang, T. Meng, D. Guo, J. Qin and M. Cao, *Angew. Chem. Int. Ed.*, 2020, **59**, 15232-15237.
2. X. Wang, G. Long, B. Liu, Z. Li, W. Gao, P. Zhang, H. Zhang, X. Zhou, R. Duan, W. Hu and C. Li, *Angew. Chem. Int. Ed.*, 2023, **62**, e202301562.
3. C. P. Wang, X. J. Liu, I. Ohnuma, R. Kainuma, K. Ishida and S. M. Hao, *J. Phase Equilib.*, 2000, **21**, 54-62.
4. N. Lu, Y. Liang, C.-Y. Ren, X. Liang, Y.-C. Zhang, X.-D. Zhu and J. Gao, *J. Mater. Chem. A*, 2024, **12**, 1852-1861.
5. L. Meng, S. Shang, S. Liu, L. Zhang, Q. Tang, H. Wang, F. Wang, C. Li, Y. Sun and H. Wu, *Applied Catalysis B: Environment and Energy*, 2024, **358**.
6. D. Jin, X. Liu, J. Cao, M. Wei, X. Liu, Y. Chen, X. Li, Q. Wu, Z. Dong and H. Liu, *Int. J. Hydrogen Energy*, 2024, **110**, 617-627.
7. P. Zuo, X. Ji, J. Lu, Y. Chai, W. Jiao and R. Wang, *J. Colloid Interface Sci.*, 2023, **645**, 895-905.
8. J. Wang, M. Zhang, G. Yang, W. Song, W. Zhong, X. Wang, M. Wang, T. Sun and Y. Tang, *Adv. Funct. Mater.*, 2021, **31**, 2101532.
9. J. Sun, F. Guo, X. Ai, Y. Tian, J. Yang, X. Zou and G. Zhu, *Small*, 2023, 2304573.
10. Y. Gu, A. Wu, Y. Jiao, H. Zheng, X. Wang, Y. Xie, L. Wang, C. Tian and H. Fu, *Angew. Chem. Int. Ed.*, 2021, **60**, 6673-6681.
11. X. Jian, W. Zhang, Y. Yang, Z. Li, H. Pan, Q. Gao and H.-J. Lin, *ACS Catal.*, 2024, **14**, 2816-2827.
12. H. Peng, K. Zhou, Y. Jin, Q. Zhang, J. Liu and H. Wang, *Chem. Eng. J.*, 2022, **429**, 132477.
13. Y. Luo, S. Wu, P. Wang, H. Ranganathan and Z. Shi, *J. Colloid Interface Sci.*, 2023, **648**, 551-557.